Design and optimization of an Al doped ZnO in Si-slot for gas sensing

Ritapa Bhattacharjee, N.T. Kejalakshmy, B.M. Azizur Rahman, Fellow, IEEE

City University of London, London, EC1V0HB, United Kingdom

Abstract: A Silicon waveguide incorporating a vertical slot filled with Al^{+3} doped ZnO is proposed for gas sensing. The effect of different device parameters, namely, slot-height, slot-width and Si-width on two key optical features related to sensing, that is, difference in effective index and differential modal loss, before and after the exposure to gas are investigated using a fully-vectoral finite element method. The optimized sensor with a slot height of 400 nm, slot width of 100 nm and Si width of 65 nm yields the effective index difference of ~0.285 and differential loss ~4.35 dB/μm, indicating a viable device for gas sensing applications. Detailed numerical analyses also reveal that, at some structural parameters, two anti-crossing modes appear which can significantly alter the device performances and thus should be avoided.

Index Terms: Slot waveguide, Sensors

1. Introduction

Recently, demand of gas sensors has considerably increased owing to increase in the environmental pollutants and industrial wastes, along with the public awareness and desire to make our environment better and safer. Preferences are given to sensors with small size, high sensitivity, and low power consumption at a lower price [1]. Gas sensors based on metal oxides are widely used in the detection of various toxic gases causing pollutions [2,3]. Amongst these, Zinc oxide (ZnO) based sensor has received much attention due to its change in resistivity for a particular gas with a high selectivity [4]. Various doped and undoped ZnO sensors in the form of bulk, thick-film, thin-film, nano-powder, nano-rod, nanowire, etc. have been considered for sensing applications, such as, determining freshness of sea food, toxic gases like ethane, carbon dioxide, nitrogen oxides, etc. [4-8]. The doping concentration and the structural morphology of such oxides determine the sensitivity and selectivity of all these sensors. In a nano-sized sensor with its larger surface-to-volume ratio, the interaction with the sensing object is larger compared to the bulk sensors, leading to increased sensitivity and reduced operating temperature [9-11].

ZnO is an n-type direct band semiconductor with a very wide bandgap. The Oxygen vacancies on the surface of metal oxides work as n-type donors and increase the oxide's conductivity. In case of oxidizing gases such as NO_2, O_2 etc., the electrons get depleted effectively from the conduction band, resulting in the reduction in conductivity of n-type oxides. But in case of reducing gases like NH_3, CO, H_2, alcohols, etc., conductivity increases due to increase in conduction electrons and oxygen vacancies [4,5].

Recently, slot waveguides are becoming very attractive for sensing applications [12-14]. The slot waveguide with a low refractive index in the very narrow slot region is capable of a very high light confinement in this area. The small size in the order of a few tens of nanometre has also the advantage of using them as sensors. They are highly sensitive to change in refractive index of the slot or change in thickness of the deposited receptor layers [12]. Various types of biosensor and chemical sensors incorporating slot waveguide have been reported [13-16], including an investigation on ammonia gas detection with nitride-on-silicon slot waveguide by using the absorption technique [17].

Aluminium doped ZnO thin films have shown a very large change in resistance while sensing ammonia, which is a gas of reducing nature [5]. Recently an Al^{+3} doped ZnO (AZO) coated Au nanowire has been studied by using the finite element method (FEM) for gas sensing [18]. In this paper, the concept of AZO nanosensors for sensing gases of reducing nature is considered for the design and optimisation of a new type of slot waveguide sensor incorporating AZO on silicon.
A full-vectorial FEM, as given in Eq. (1), is used to obtain modal solutions of the slot waveguides [19, 20]:

$$\omega^2 = \frac{\int\left[(\vec{\nabla}\times\vec{\mathrm{H}})^* \varepsilon^{-1} (\vec{\nabla}\times\vec{\mathrm{H}}) + \mathrm{p}\,(\vec{\nabla}\cdot\vec{\mathrm{H}})^* (\vec{\nabla}\cdot\vec{\mathrm{H}})\right] dx\,dy}{\int \vec{\mathrm{H}}^*\cdot\mu\ \vec{\mathrm{H}}\ dx\,dy} \quad (1)$$

Here, $\vec{\mathrm{H}}$ is the magnetic field and * denotes the complex conjugate and transpose. In the numerical simulation, ω^2 is the eigenvalue where ω is the angular frequency of the wave, μ is the permeability and ε is the permittivity, and p is the dimensionless penalty parameter to eliminate spurious modes.

Doping of ZnO with Al_2O_3 effectively replaces the Zn by Al atoms and thus increases the conductivity of ZnO [21]. The plasmonic frequency can be incorporated in the material model by using the Lorentz-Drude model as given below [12, 22],

$$\varepsilon_\omega = \varepsilon_{ZnO} - \frac{\omega_p^2}{\omega_p^2 + j\gamma\omega} \quad (2)$$

In Eq.2 ε_{ZnO} is the dielectric constant of ZnO. The contribution of free electron or plasmon is given by the second term. The plasma frequency, ω_p, is given by, $\omega_p = Ne^2/\varepsilon_\circ m^*$ and carrier damping constant, $\gamma = e / \mu m^*$. Here e denotes the electron charge and $\varepsilon_\circ$ static dielectric constant. The grain size of Al-doped ZnO (AZO) is considered to be 20 nm, the corresponding carrier concentration, N, is taken as 6.2×10^{20} cm^{-3} and mobility, μ, as 25 cm^2/Vs [23]. The doping concentration of Al is taken as 3.6% and the effective mass, m^*, is considered as 0.28 times the mass of the electron [23]. We consider that a reducing gas depletes the carrier concentration by 90% [18]. Therefore, the values of real and imaginary part of relative permittivity of AZO with exposure to gas are computed with carrier concentration in the order of 10^{19}.

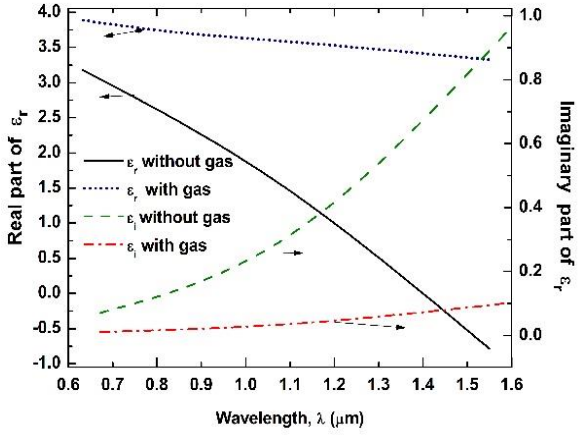

Fig.1. Variation of relative and imaginary parts of permittivity with the wavelength before and after gas exposure.

Figure 1 shows the variations of the real and imaginary parts of the relative permittivity, ε_r, of AZO with the wavelength. For an efficient slot waveguide sensor to be ~~a~~ viable, the differential loss in the waveguide before and after gas exposure, needs to be optimised. At 800 nm wavelength, imaginary parts of the refractive indices are 0.04256 and 0.00447 before and after exposure to gas, respectively, which are very small compared to other wavelengths, yet the differential loss is considerably high which indicates the possibility of making a low-loss device. This wavelength is also easily available with a Ti-Sapphire laser. So, we consider 800 nm as the probe wavelength for the optimisation of the slot waveguides. During electrical measurements, the grain boundary prevents the hopping of surface electrons within the Debye length for nano-sized materials and thus interferes in the sensing measurement. Whereas, in the case of bulk materials, the material under Debye length basically remains electrically inactive. Hence, in the case of nano-sized sensor device, it would be more preferable to consider optical parameters as electrical characteristics are not suitable due to the boundary effect.

When carrier concentration, N increases the effective index of the doped ZnO filled slot guide reduces, however its modal loss is increased. Here, we focus on two key optical parameters characterising the performance of the slot waveguide as a sensor. These are the difference in their effective indices (Δn_{eff}) and differential loss ($\Delta\alpha$), respectively, before and after exposure to gas and are defined as follows:

$$\Delta n_{eff} = |n_{eff}(N_a) - n_{eff}(N_b)| \quad (3)$$

$$\Delta\alpha = |\alpha(N_a) - \alpha(N_b)| \quad \text{in dB/mm} \quad (4)$$

Here in Eq.3, $n_{eff}(N_a)$ and $n_{eff}(N_b)$ are the effective indices of the slot waveguide before and after exposure to gas, respectively and in Eq.4, $\alpha(N_a)$ and $\alpha(N_b)$ are the modal losses before and after gas exposure, respectively. N_a and N_b denote the carrier
concentration of AZO before and after the gas exposure. The aim of this work is to increase both Δn_{eff} and $\Delta\alpha$ and to have a low $\alpha(N_b)$ value for a viable gas sensing device with AZO slot waveguide.

2. Slot Design

The schematic of AZO filled Si slot waveguide is shown in Fig.2. Here, W represents the width of each Si-slab, H represents the height of each Si-slab, which also defines the slot height and W_s represents the slot width. Here, the refractive indices of Si and SiO_2 are taken as 3.882 and 1.457, respectively, at the operating wavelength of 800 nm. The refractive index of AZO before and after exposure to gas are considered as 1.61839 and 1.93571, respectively. The thickness of AZO layer in the cover medium surrounding Si-slab is taken as 50 nm.

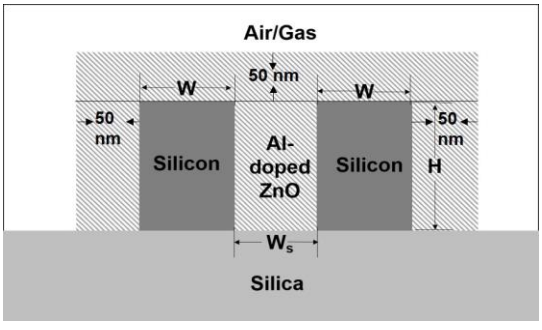

Fig. 2. Schematic of the cross-sectional view of the Slot waveguide.

There are two possible fundamental quasi-TE (H_{11}^{y}) and quasi-TM (H_{11}^{x}) modes, which can be guided through this waveguide. The H_{11}^{x} mode has dominant H_x and E_y components and both of them are continuous across the slot-interface. On the other hand, although dominant H_y component of the H_{11}^{y} mode is continuous, but its dominant E_x component is not continuous across the slot interface. The boundary condition forces E_x component to increase in the low-index slot region and thus yields a high power confinement in the low-index slot region. Figure 3(a) shows the contour plot of E_x modal field of the fundamental quasi-TE H_{11}^{y} mode with H = 400 nm, W = 65 nm and W_s = 60 nm before exposure to gas and Fig.3(b) shows the variation of the dominant electric field intensity (E_x) along the x-axis.

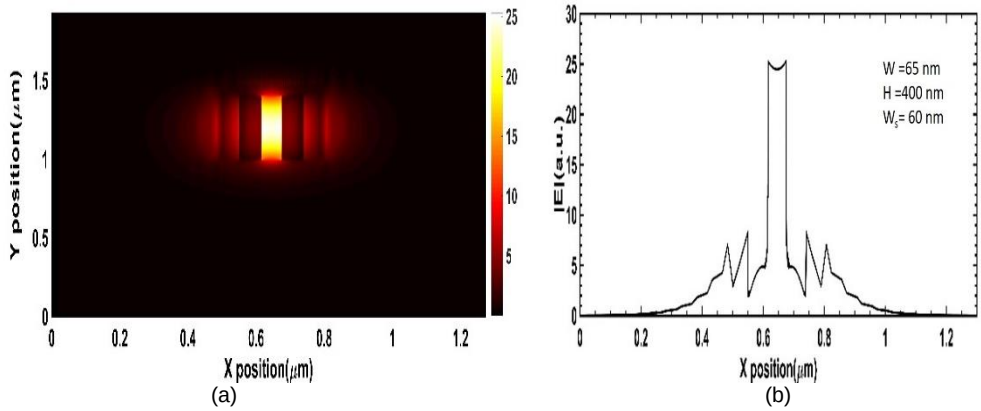

(a) (b)

Fig. 3. (a) Contour plot of E_x modal field in the slot region, (b) E_x field intensity along the x-axis.

From Fig. 3(a) we can observe that the E_x field is well confined in the low index AZO slot in between the two Si-slabs shown by lighter yellow colour. From the Fig. 3(b), it can be observed that the peak field intensities appear at the edges due to change in material. The Intensity however remains maximum in the AZO slot region.

The confinement factors in the slot, Γ_s, and the Si slabs, Γ_{si}, are defined as follows:

$$\Gamma_s = \frac{\iint_{S} |E(x,y)|^2 \, dxdy}{\iint_{\infty} |E(x,y)|^2 \, dxdy} \qquad \Gamma_{si} = \frac{\iint_{si} |E(x,y)|^2 \, dxdy}{\iint_{\infty} |E(x,y)|^2 \, dxdy} \quad , \tag{5}$$

In Eqn. 5 the ***E*** *(x, y)* is the electric field vector and S and Si below the integrator signs in the numerator indicate that integrations are carried out in the slot and silicon core regions, respectively and for the denominator over the entire waveguide region is considered.

3. Analysis of AZO on Si slot for gas sensing

First, variations of the confinement in silicon slab with the width, W for different heights, H are studied. Initially the W_s is kept fixed at 60 nm. Variations of the confinement factors in Si-slab are shown in Fig.4 with the slab width, W for different H values. With increase in W, the confinement factor in the Silicon core increases. Similarly, increase in the H also increases the confinement factor. Waveguide with a larger Si-dimension confines more light in the high index Si region and the confinement factor tends to reach unity for their very large values.

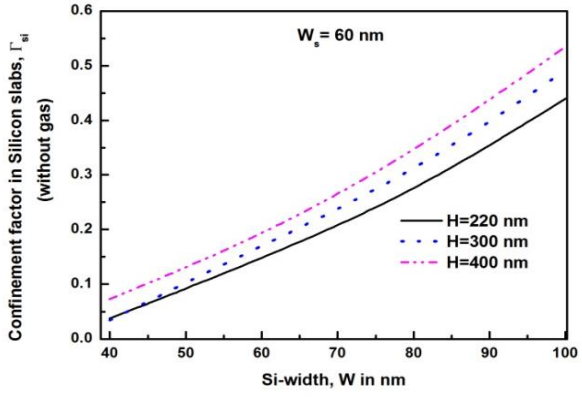

Fig. 4. Variations of the power confinement in Si-slabs with the Si-width.

Variations of effective index with the W are shown in Fig.5 when W_s is fixed at 60 nm. The effective index increases with increase in W, as more light is confined in the high-index Si-core. Similarly, effective index also increases as the height H is increased. This is expected, as the dimensions of silicon slabs are increased, more light gets confined in the higher index silicon slabs as shown in Fig.4, and thus, resulting in the increased effective indices. Next, variation of the confinement factor in the slot region with the Si-width is studied.

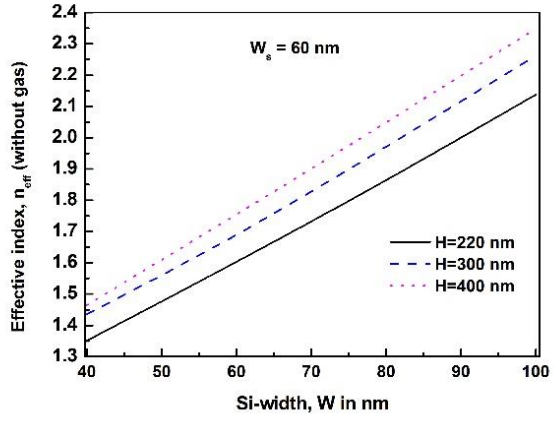

Fig. 5. Variation of effective index with Si-width.

Variations of power confinements in the slot with the Si-slab width are shown in Fig. 6. Here, it can be observed that the confinement factor increases with decrease in W and reaches a maximum peak and then decreases as W is reduced further. Initially, as W reduces less light is confined in Si-slab layer, as shown in Fig.4, and so power in the slot area increases. However, on further reduction of W, the confinement factor in the slot reduces as the mode approaches it's cut off, the power moves in the lower SiO_2 buffer layer. It can be noted that the maximum confinement factor is higher with the increase in H and also appears at a slightly lower value of W.

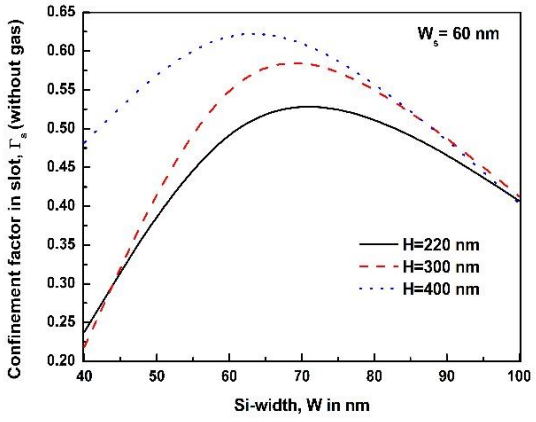

Fig. 6. Variation of confinement in Slot with Si-width.

Next, variations of modal loss values with the absence of gas for different W and H values are shown in Fig. 7. Here, all the materials are considered to be loss-less except AZO and the modal loss arises due to light confinement in this region only. However, if needed, dielectric loss from other materials or scattering loss can also be included in the final design. Figure 7 shows the variation of modal loss with *W* for different values of H for a fixed W_s = 60 nm. The modal loss increases with increase in W and attains a peak value at around 65 nm for all the different H values considered here and then reduces, which correlates very well with the power confinement in the slot region.

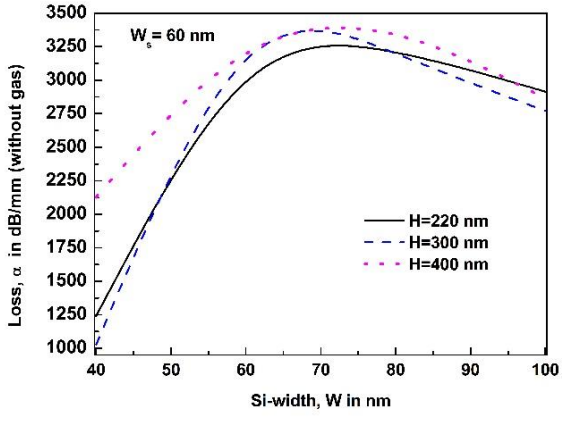

Fig. 7. Variation of loss in dB/mm with Si-width without gas exposure.

Variations of the effective index and confinement factor after exposure to gas are also studied. In the presence of gas, the real and imaginary parts of AZO refractive indices are taken as 1.93571 and 0.004470, respectively and with the absence of gas are taken as, 1.61839 and 0.04256, respectively. Both the effective index, confinement factor of this slot guide after exposure to gas are not shown here, but they show similar behaviour with the structural parameter variation without exposure to gas, as shown earlier. However, when gas is introduced, as the imaginary part of the refractive index reduces which results in nearly 10 times lower loss compared to that in the absence of gas. Figure 8 shows the variation of Loss in dB/mm with W for different H after the gas exposure.

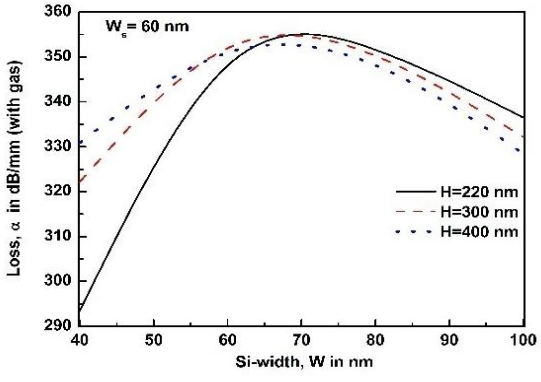

Fig. 8. Variation of Loss in dB/mm with Si-width with gas.

Next, in Fig.9 variation of effective index with W_s is shown for different H values with W = 65 nm. The effective index reduces with increase in W_s. The slot mode can be considered as the even-supermode of two coupled Si-slab with W_s as the separation between them. So, similar to a directional coupler problem, the effective index of the even-supermode decreases with the separation (here slot width, W_s) between the two waveguides. The effective index is bigger for higher Si-height, as the effective index of the isolated mode is also larger.

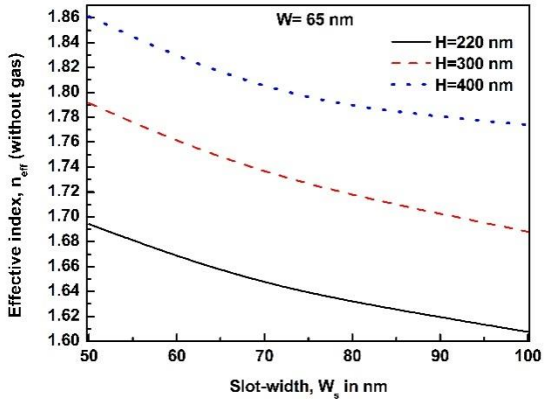

Fig. 9. Variation of effective index with the slot width, W_s.

In Fig.10, variations of differential loss, Δα before and after gas exposure with W_s for different H are plotted. When H = 300 nm, the Δα is apparently constant, however, for H = 400 nm, the differential loss, Δα increases with the W_s. On the other hand, for H = 220 nm, the Δα goes through an apparently random behaviour.

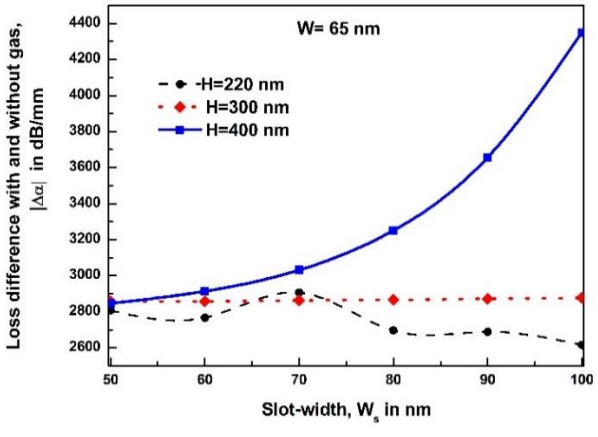

Fig. 10. Variation of differential loss in dB/mm with slot-width.

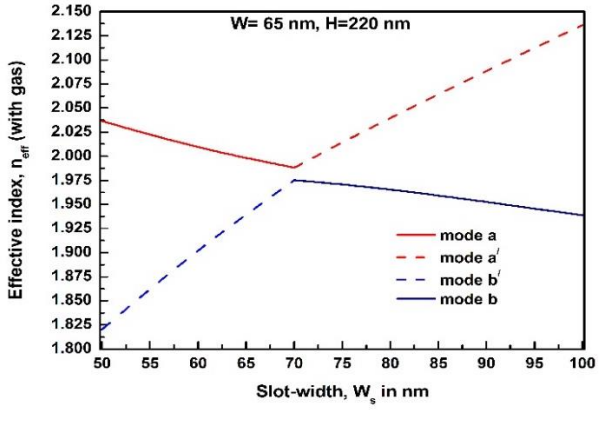

Fig. 11. Variation of effective index for modes a and b with slot width for a slot height of 220 nm.

To look at this issue closely, we have studied evolution of modes, and particularly for this case, we have followed other modes close to this slot mode. It can be observed from Fig.11 that, in this case two guided modes appear in this region. One mode for which effective index reduces (as shown by solid lines) with increase in W_s, this is similar as the even supermode which
reduces with the separation between the guides. But it appears that there is another mode for which the effective index increases (as shown by dashed lines) with increase in W_s. This causes degeneracy of the modes, when they go through the

anti-crossing point. As the modal losses of these two modes are different, the loss value as shown by dotted curve with circles in Fig.10 for H = 220 nm, shows an increase when the slot width was close to 70 nm_. In Fig.10, if we remove this anomalous point of W_s = 70 nm, then the loss difference curve shows a clear slope of loss reduction for H = 220 nm. We did notice similar degeneration of modes when slab height was 500 nm, and that is why we did not present results for this particular case even though, localised differential loss could be higher, but performance as a sensor could be more unpredictable.

4. Optimization of Slot structural parameters

The prime motivation of this work was to achieve optimized structural parameters of AZO slot waveguide with highest Δα and Δn_{eff}. From the analysis of AZO the best Δα appears at a H = 400 nm. Also, with H = 400 nm, the anomalies in the effective index are not significant compared to the case of a higher (e.g., H = 500 nm) or lower height (e.g., H = 220 nm). For W= 65 nm, the confinement factor appears to be highest after the gas exposure (68.06 %) and with W_s = 100 nm, the highest Δα has been achieved. With these structural parameter values, H = 400 nm, W = 65 nm and W_s =100 nm of the AZO slot waveguide, the Δn_{eff} and Δα are obtained as 0.285 and 4.349 dB/μm, respectively. The loss after exposure to gas for this structure has been computed as 3.562 dB/μm and the propagation length, L_p (L_p= -10log$_{10}$(1/e)/α), as 12.191 μm.
To achieve a phase difference, equal to π, the required propagation length is $L_\pi = \lambda/2\ \Delta n_{eff,}$ and in this case with Δn_{eff} = 0.285, the L_π value is 1.40 μm. On the other hand, to have a differential loss, ΔαL = 20 dB, the required length, L should be 4.60 μm. In this case, the total loss with exposure to gas is only 1.637 dB and when not exposed to gas is 21.637 dB. This indicates the AZO slot waveguide can be a viable sensing device with an acceptable loss. The AZO slot waveguide is promising when used as single waveguide sensor compared to when arranged in a Mach-Zehnder based sensor arrangement. Because although in one state (with no phase difference) losses will be low in both the branches of the Mach-Zehnder arms, however for other state, when the required phase difference is π is achieved, the sensing branch will suffer a loss of 4.5 dB. In that case, even the two fields will have a π phase difference, but they will not cancel each other, as their magnitudes are significantly different.

Therefore, to achieve high Δα, the AZO slot waveguide is optimized for a gas sensor of 4.6 μm long with W = 65 nm, H = 400 nm, W_s =100 nm to provide 20 dB differential loss with only 1.64 dB insertion loss. Next, effect of possible fabrication tolerances is studied and shown in Table 1. For W_s = 100 ± 10nm, that is for W_s of 90 nm and 110 nm, the α, after exposure to gas are calculated as, 0.352 dB/μm and 0. 360 dB/μm, respectively and this yields the differential loss, Δα as, 3.656 dB/μm. and 5.313 dB/μm, respectively. Below W_s of 100 nm the Δα reduces a bit but would yield better than 20 dB differential loss when W_s is increased. For the case of W = 65 ± 5 nm that is, at 60 nm and at 70 nm, we have calculated α after exposure to gas as 0.351dB/μm and 0.362 dB/μm, Δα as 3.506dB/μm and 5.652 dB/μm, respectively. The Δn_{eff} values are also shown as 0.296 and 0.263, respectively. For H = 400 ± 50 nm, that is at 350 nm and at 450 nm, the values of α, Δα, Δn_{eff} are obtained as, 0.350 dB/μm and 0.375 dB/μm, 3.136 dB/μm and 6.821dB/μm, 0.302 and 0.197, respectively. These studies show that performance of the gas sensor will be stable with possible change in its width, height or slot width, which can happen during the fabrication process. However, if we want to make sure of minimum 20 dB differential loss against slightly reduced differential loss values, a slightly larger device would be adequate. The slot structure designed here can be easily fabricated by well-developed standard CMOS technology used by the semiconductor industries [24]. In Table1 we have listed the values of α, Δα and Δn_{eff} with respect to possible variation in the H, W and W_s.

Table 1: Tolerances of different parameters

H (nm)	W (nm)	W_s (nm)	α dB/μm	Δα dB/μm	Δn_{eff}
400	60	100	0.386	3.506	0.296
400	70	100	0.601	5.652	0.263
400	65	90	0.352	3.656	0.296
400	65	110	0.360	5.313	0.269
350	65	100	0.350	3.136	0.302
450	65	100	0.375	6.821	0.197

5. Conclusions

An Al^{+3} doped ZnO on Silicon slot waveguide is designed and analysed for gas sensing. For some structural parameters of the slot waveguide a few modal anomalies appeared with anti-crossing mode, which reduce the effective index difference or differential loss or both before and after exposure to gas. To achieve high effective index difference along with high differential loss by carefully avoiding the structural parameters with significant possibilities of modal anomalies, key

parameters of the

slot waveguide are taken as, slot width of 100 nm, slot height of 400 nm and silicon-slab width of 65 nm. At these structural parameters, the Al^{+3} doped ZnO on Silicon slot waveguide shows a promising result with its effective index difference as 0.285 and differential loss as 4.35 dB/μm. This indicates the possibility of a compact 4.6 μm long Al^{+3} doped ZnO based Silicon slot waveguide sensor yielding 20 dB differential loss and Insertion loss value of only 1.637 dB.

Acknowledgements

RB thanks to Erasmus Mundus INTACT postdoctoral mobility fellowship from Asia to EU for funding her during this project.

References

[1] B. Timmer, W. Olthuis, and A.van den Berg, “Ammonia sensors and their applications—a review,” Sensors and Actuators B vol.107, pp. 666–677 2005.
[2] C. Wang, L. Yin, L. Zhang, D. Xiang, and R. Gao, “Metal oxide gas sensors: Sensitivity and influencing factors,” Sensors, vol.10, no. 3, pp. 2088-2106, 2010.
[3] Y.F. Sun, S.B. Liu, F.L. Meng, J.Y. Liu, Z. Jin, L.T. Kong, and J.H. Liu, “Metal oxide nanostructures and their gas sensing properties: a review,” Sensors, vol.12, no. 3, pp. 2610-2631, 2012.
[4] S.M. Chou, L.G. Teoh, W.H. Lai, Y.H. Su, and M.H. Hon, “ZnO: Al thin film gas sensor for detection of ethanol vapor,” Sensors, vol. 6, pp. 1420-1427, 2006.
[5] H. Nanto, T. Minami, and S. Takata, “Zinc-oxide thin film Ammonia gas sensor with high sensitivity and excellent selectivity,” J. App. Phys, vol 60,pp. 482-484, 1986.
[6] N.L. Hadipour, A.A. Peyghan, and H. Soleymanabadi, “Theoretical study on the Al-Doped ZnO nanoclusters for CO chemical sensors,” Phys. Chem. C vol. 119, pp. 6398−6404, 2015.
[7] N. Hongsith, E. Wongrat, T. Kerdcharoen, and S. Choopun, “Sensor response formula for sensor based on ZnO nanostructures,” Sensors and Actuators B, vol. 144, pp. 67–72, 2010.
[8] H. Nanto, H. Sokooshi, and T. Kawai, “Aluminum-doped ZnO thin film gas sensor capable of detecting freshness of sea foods,” Sensors and Actuators B, vol. 13, no. 14, pp. 715-717, 1993.
[9] O. Lupan, V.V. Ursaki, G. Chai, L. Chow, G.A. Emelchenko, I.M. Tiginyanu, A.N. Gruzintsev, and A.N. Redkin, “Selective hydrogen gas nanosensor using individual ZnO nanowire with fast response at room temperature,” Sensors and Actuators B: Chemical, vol. 144, no. 1, pp. 56-66, 2010.
[10] J.J. Hassan, M.A. Mahdi, C.W. Chin, H. Abu-Hassan, and Z. Hassan, “A high-sensitivity room-temperature hydrogen gas sensor based on oblique and vertical ZnO nanorod arrays,” Sensors and Actuators B: Chemical, vol. 176, pp. 360-367, 2013.
[11] S.P. Chang and K.Y. Chen, “UV illumination room-temperature ZnO nanoparticle ethanol gas sensors,” ISRN Nanotechnology, 453517, 2012.
[12] F. Dell ‘Olio and V.M.N. Passaro, “Optical sensing by optimized silicon slot waveguides,” Opt. Express, vol. 15, no. 8, pp. 4977-4993, 2007.
[13] J. T. Robinson, L. Chen, and M. Lipson, “On-chip gas detection in silicon optical microcavities,” Opt. Express, vol.16, pp. 4296-4301, 2008.
[14] V.M.N. Passaro, M. La Notte, B. Troia, L. Passaquindici, F. De Leonardis, and G. Giannoccaro, “Photonic structures based on slot waveguides for nanosensors: state of the art and future developments,” Int. J. of Res. and Rev. in App. Sci., vol. 11, no. 3, pp. 411-427, 2012.
[15] C. Pan, and B. M. A. Rahman, “High-sensitivity polarization-independent biochemical sensor based on silicon-on-insulator cross-slot waveguide,” IEEE J. Sel. Topics Quantum Electron, vol. 23, no. 2, pp. 64-71, 2017.
[16] S. Ghosh and B. M. A. Rahman, “An innovative straight resonator incorporating a vertical slot as an efficient bio-chemical sensor,” IEEE J. Sel. Topics Quantum Electron., vol. 23, no.2, pp.132–139, 2017.
[17] B. Kumari, A. Barh, R.K. Varshney, and B.P. Pal, “Silicon-on-nitride slot waveguide: A promising platform as mid-IR trace gas sensor,” Sensors and Actuators B: Chemical, vol. 236, pp. 759–764, 2016.
[18] N.T. Kejalakshmy, K.T.V. Grattan, and B.M.A. Rahman, “Investigation of the optical modal properties of Al^{+3} doped ZnO-coated Au waveguide for gas sensing applications using the finite element method,” IEEE Sensors J.vol.16, no.5, pp.1176-1121, 2016.
[19] B.M.A. Rahman and J.B. Davies, “Penalty function improvement of waveguide solution by finite elements,” IEEE Trans. Microw. Theory Techn., vol 32, no.8, pp. 922-928, 1984.
[20] C. Themistos, B.M.A. Rahman, and K.T.V. Grattan, “Finite element analysis for lossy optical waveguides by using perturbation techniques,” IEEE Photon. Technol. Lett., vol.6, no.4, pp. 537-539, 1994.
[21] C. Agashe, O. Kluth, J. Hùpkes, U. Zastrow, B. Rech, and M. Wuttig, “Efforts to improve carrier mobility in radio frequency sputtered aluminum doped zinc oxide films,” J. Appl. Phys., vol.95, no. 4, pp.1911-1917, 2004.
[22] J. Han, Z. Zhu, S. Ray, A.K. Azad, W. Zhang, M. He, S. Li, and Y. Zhao “Optical and dielectric properties of ZnO tetrapod structures at terahertz frequencies,” Appl. Phys. Lett., vol 89, 031107, 2006.
[23] S. Cornelius and M. Vinnichenko, “Al in ZnO - from doping to alloying: An investigation of Al electrical activation in relation to structure and charge transport limits,” Thin Solid Films, vol. 605, pp. 20-29, 2016.
[24] A. Säynätjoki, L. Karvonen, T. Alasaarela, X. Tu, T. Y. Liow, M. Hiltunen, A. Tervonen, G. Q. Lo, and S. Honkanen, "Low-loss silicon slot waveguides and couplers fabricated with optical lithography and atomic layer deposition," Opt. Express, vol.19, pp. 26275-26282, 2011.